AIAA JOURNAL
Vol. 40, No. 3, March 2002

Computational Study of Intake Duct Effects on Fan Flutter Stability

M. Vahdati,* A. I. Sayma,* C. Bréard,† and M. Imregun‡
Imperial College of Science, Technology, and Medicine, London, England SW7 2BX, United Kingdom

A detailed flutter analysis is presented of a civil aeroengine fan assembly using an integrated three-dimensional aeroelasticity model. Two different intake ducts are considered. The first one is a straight duct, the geometry of which is representative of test rig intakes. The second duct is an axisymmetric version of the flight intake. During the first phase of the study, a series of flutter analyses was conducted for the 60–80% speed range. Each computation was performed at a single point along the speed characteristic by following an elevated working line that was near the expected flutter boundary. As routinely observed in rig tests, the flutter stability was predicted to drop sharply for some very narrow speed ranges, but the behavior was found to be markedly different for each individual intake. To gain further understanding of the intake effects, a large number of calculations were undertaken for the second intake alone. An assumed pressure perturbation, due a rotating fan assembly vibrating in a given nodal diameter mode, was imposed at the duct exit. The propagation of this perturbation was monitored at a number of stations along the duct. The cases studied were chosen to cover the combinations of speeds and nodal diameters for which the earlier fan assembly plus intake calculations had predicted flutter. It was shown that, for a given nodal diameter assembly mode, instabilities occurred when the perturbation frequency was sufficiently close to the duct's cuton frequency in the region close to the fan. Such a finding suggests that fan flutter and intake duct acoustics are related in an integral fashion. Flutter will occur when the pressure perturbation due to fan rotation and blade vibration match, both in frequency and shape, an acoustic mode of the intake.

Nomenclature

A	=	prescribed maximum perturbation amplitude
m	=	circumferential wave number for acoustic mode
N	=	number of nodal diameters in vibration mode
$\bar{p}(r)$	=	amplitude of steady-state pressure
r	=	radial coordinate
t	=	time
Δp	=	unsteady pressure
Δu	=	unsteady axial velocity
θ	=	angular coordinate
Ω	=	rotational speed
ω_b	=	natural frequency of blade $1F$ mode
$1F$	=	blade first flap mode

I. Introduction

VIBRATION is a universal engineering problem, and most components, which are subjected to high-speed airflow, are also susceptible to self-excited vibration, or flutter. In turbomachinery applications, flutter is usually associated with fan blades, although other compressor and low-pressure turbine blades may also suffer from such instabilities. Indeed, there is a long history of flutter problems in the design of aeroengine fans. Whereas the need to avoid flutter to preserve fan integrity is obvious, also note that flutter is increasingly becoming a limiting factor in developing improved-efficiency designs, especially when flexible, slender, and unshrouded blades are used. In the main, fan flutter is observed in one to six forward traveling nodal diameter assembly modes, the blades usually vibrating in their first flap mode. The worst condition, for which the stability margin from the working line is smallest, typically occurs between 60 and 80% speeds. Within that interval, the flutter stability is reduced sharply for specific narrow speed ranges, hence the term flutter bite.

A recent review of turbomachinery aeroelasticity is given by Marshall and Imregun,[1] which also includes an overview of computational fluid dynamics (CFD) methods for unsteady flows. Most flutter investigations treat the fluid and the structure as two distinct media, and two separate analyses are linked via the surface pressure, which is converted to a set of sinusoidal forces and moments acting on the blade.[2,3] The flutter stability is determined by the amount of positive or negative damping exhibited by the complex eigenvalues of the aeroelastic system. A detailed frequency-domain analysis based on aeroelastic response functions is given by Imregun.[4] More advanced time-domain techniques employ a finite element representation for the structural part and reduce the mode shapes to a set of aerodynamic coordinates.[5,6] Although the governing equations are solved separately, the structural motion due to fluid forces at the current time step is used as a boundary condition to the fluid flow at the next time step and vice versa. There are no restrictions on the aerodynamic model that can be used, the only limitation being the available computing power. Such approaches allow the inclusion of most nonlinear effects, both of structural and aerodynamic origin, and the flutter behavior is deduced from convergent, limit-cycle or divergent time histories predicted at the blade surface. With advances in computational methods and faster computing hardware, full-assembly models with time-accurate aerodynamics and blade flexibility are beginning to emerge. Chew et al.[7] used such an approach to predict the flutter of a 26-bladed fan assembly and compared their results with experimental data. A major conclusion from this work was that part-speed assembly mode flutter could be predicted using an essentially inviscid unsteady model, provided the starting steady-state flow was computed on a fine viscous mesh and the steady-state losses were extrapolated to the inviscid unsteady solution. The work of Vahdati et al.[8] demonstrated the importance of retaining the viscous effects, albeit via a loss model, when dealing with separated flow flutter.

In any case, in spite of extensive research work over the past 40 years, an accurate determination of the flutter boundaries for realistic industrial configurations remains a challenging problem, especially around the flutter bite. In general terms, flutter modeling needs to capture both global characteristics and local detail. The former include suction surface boundary layer as well as the shock

Received 22 May 2000; revision received 13 August 2001; accepted for publication 13 September 2001.

*Research Fellow, Mechanical Engineering Department.
†Research Associate, Mechanical Engineering Department.
‡Professor, Mechanical Engineering Department.

position and magnitude of the steady-state flow, whereas the latter requires the modeling of small local variations, such as marginally different leading edge profiles. To complicate matters further, flutter occurs at part speeds near the stall boundary, where it is very difficult to obtain an accurate steady-state solution. Whereas the basic instability is believed to depend on the unsteady flow features and the structural behavior of the fan blade, the flutter margin is usually associated with other factors such as blade mistuning, flow distortions at the inlet, and those caused by bleeds, pylon effects, and intake duct properties. This last factor is the main topic to be studied in this paper.

Over the past 10 years or so, measurements on aeroengine test rigs and theoretical considerations have lead to the hypothesis that fan flutter may be influenced by the acoustic properties of the intake duct. It has been postulated that the variation in the cross-sectional area of the duct may cause acoustic waves from the fan to be cut-off at the intake throat, the trapped energy leading to an acoustic resonance and to greater susceptibility to fan blade flutter (private communications from C. Freeman, 1998, and A. B. Parry, 1998). A full review of intake acoustics is well beyond the scope of the present paper, but it is useful to mention some of the relevant publications. Campos and Lau[9] assumed a low Mach number and that the acoustic wavelength was negligible compared to the length scale of the cross-sectional area variation, allowing them to derive an analytical solution. Uenishi and Myers[10] used a two-dimensional modified wave energy method to represent the sound field in a nonuniform duct carrying a quasi-one-dimensional mean flow. Eversman and Astley[11] and Astley and Eversman[12] used numerical methods to consider the transmission of sound through nonuniform ducts carrying high-speed compressible flows. Nayfeh et al.[13–15] have used a mixture of analytical and numerical methods to study the acoustics of nonuniform circular and annular ducts with a range of mean flow profiles for both hard and soft wall boundary conditions. The case of rotating blade rows was investigated by Hanson,[16] who modified the flat plate cascade model of Smith[17] to accommodate two blade rows in relative motion. His results showed that acoustic mode trapping could occur in such situations. In any case, accurate predictions of aeroengine forward-arc noise require not only a realistic representation of the intake duct with finite length and significant asymmetry, but also the inclusion of the rotating fan blades. When dealing with the intake only, the acoustic modes can be computed in the frequency domain using a linearized finite/infinite element velocity potential formulation.[18] It is assumed that an irrotational isentropic acoustic disturbance propagates through a prescribed irrotational mean flow without interacting with it. A review of infinite elements for wave problems is given by Astley[19] with emphasis on accuracy and the use of high-order hierarchical shape functions.

With dramatic increases in computing power, CFD-based methods are increasingly being used for the investigation of duct acoustics. For instance, three-dimensional nonlinear CFD calculations have already been reported by Ozyoruk and Long,[20,21] who studied ducted fan noise. Near-field acoustics were determined via the Euler equations, whereas far-field noise was calculated using a moving surface Kirchhoff formula. A combined fan plus intake calculation was reported by Chew et al.,[7] who used an axisymmetric representation for the intake. They showed that the intake was instrumental in coupling the fan blade flutter modes, and they noted considerable acoustic activity within the intake. This particular theme will be explored further in this paper. One of the first attempts to generate and propagate duct acoustic modes for a realistic three-dimensional configuration is reported by Rumsey et al.[22] They used a Navier–Stokes code for modeling the rotor–stator interaction, a finite element based code for duct propagation, and a Kirchhoff-type code for far-field propagation.

Acoustic liners are frequently used in intake ducts to reduce noise and might also have some effect at the flutter frequencies by absorbing the wave energy and, hence, perhaps increasing the flutter margin. The modeling of acoustic liners has itself been subject to considerable research.[23,24] Here, the acoustic liner effects will be ignored on the basis that these are designed to absorb energy at frequencies that do not necessarily coincide with flutter frequencies. However, such features can be incorporated into the flutter model described in this work by using the advanced liner model of Sbardella et al.[25]

The aim of this paper is to explore the synergy between fan blade flutter and intake duct acoustics, two seemingly different areas that have not been considered together before. A specific objective is to provide an explanation for the so-called flutter bite by modeling the duct acoustics, the vibration of the fan assembly, and the unsteady flow using a large time-domain numerical model. Such a full analysis, where all relevant engineering features are modeled in a unified fashion, is seen to be the only way forward because it is more than likely that allowable simplifications will come from a better understanding of the physics and not the other way round.

II. Overview of Flutter Prediction Methodology

The details of the Imperial College aeroelasticity code AU3D have already been described by Vahdati and Imregun[26] and Sayma et al.,[27,28] who also considered several validation cases. A detailed flutter study is reported by Vahdati et al.,[8] where results from several approaches are compared against measurements obtained from an actual flutter rig. Although an overview of the aeroelasticity modeling methodology will be given subsequently for the sake of completeness, the interested reader should consult Refs. 8 and 26–28.

The flow domain is described using general unstructured grids of three-dimensional elements such as tetrahedra, hexahedra, and wedges, a feature that offers great flexibility for modeling complex shapes. The individual elements can have any number of boundary faces, and the flow variables are stored at the vertices. The numerical scheme is second-order accurate in space for tetrahedral meshes. For prismatic and hexahedral cells, the scheme is still second-order accurate for regular cells with right angles. In the worst case of a highly skewed cell, the scheme will reduce to first-order accuracy. However, hexahedral meshes are usually generated in boundary layer, where orthogonality results in regular cells. Similarly, prismatic cells are usually generated in a structured manner by projecting triangular meshes on radial layers and then connecting them. Highly skewed meshes are unlikely to occur in these situations.

The time stepping is done in an implicit fashion and, hence, very large CFL numbers can be used without creating numerical instabilities in the solution algorithm. The so-called dual time stepping is used for unsteady calculations. The time accuracy is guaranteed by the outer iteration level, where the time step is fixed throughout the solution domain, whereas the inner iterations can be performed using traditional acceleration techniques such as local time stepping and residual smoothing. A discussion of the efficiency and accuracy of viscous unsteady flow computations with dual time stepping is given by Rumsey et al.[29] They considered a biconvex airfoil and conducted several numerical studies with emphasis on mesh density and turbulence modeling.

The current aeroelasticity code can be run in viscous mode via Reynolds-averaged Navier–Stokes equations with Baldwin–Barth, Spalart–Allmaras or q-zeta turbulence models. It can also be run in inviscid mode, in which case the viscous losses are approximated using a distributed loss model. In general, a loss model assumes that the effect of the shear stresses on the motion can be represented by a distributed friction force, with the resulting flow representation still of inviscid nature, but not isentropic. The success of the loss model in approximating the true viscous flow will largely depend on the definition of the distributed friction force. The simplest representation consists of an averaged shear stress formulation using semi-empirical data, such models being commonly used for multistage turbomachinery flows in connection with quasi-three-dimensional approximations. The loss model is obtained numerically by matching two steady-state solutions for the same blade passage, the first one being computed on the standard inviscid mesh and the second one on a fine viscous mesh. The viscous solution is then interpolated onto the inviscid mesh, which is used for the analysis of the whole assembly. The viscous stresses of the first solution are, thus, saved on the second mesh and used throughout the unsteady inviscid solution as source terms.[30] Such an approach will also be used here for the fan assembly plus intake duct calculations.

The structural part of AU3D uses a modal model obtained from a three-dimensional finite element representation. It is inherently assumed that the structural behavior is linear and that the amplitude is small compared to the blade's chord. The mode shapes are interpolated onto the fluid mesh; hence, velocities and displacements

can be calculated without interpolation during the coupled motion. The equations are advanced in time using the Newmark-β method, which is unconditionally stable. During the course of the aeroelastic computations, the mesh is moved dynamically at each time step to adapt to the instantaneous shape and position of the deformed structure. The information exchange between the two domains is, therefore, achieved via pressures and displacements.

III. Definition of the Case Study

A. Preliminaries

The influence of the intake type on flutter stability has been known for sometime through rig tests of development engines. Here the aim is to study the same fan assembly with two different intakes to see whether a similar behavior can be reproduced using a large numerical model. It was decided to sweep the 60–80% speed range with a 2% speed increment so that sharp stability drops, if any, could be captured. It was decided to consider two symmetric intakes: a test rig duct (intake 1) and an axisymmetric version of the flight intake (intake 2), the respective geometries shown in Fig. 1. The fan assembly plus intake 1 will be called configuration 1, and configuration 2 is defined in the same way using intake 2. The simplification of the intake 2 geometry allows the use of an inviscid flow representation with a loss model because this particular approach is valid for symmetric assemblies only. Although a general viscous flutter analysis of the actual flight intake is possible, this route was considered to be very expensive because of the large number of runs that must be undertaken to pinpoint the critical speeds. However, a small number of viscous flutter analyses were undertaken to check the validity of the inviscid flow plus loss model approximation.

B. Discretization of the Flow Domain

The fan blade was discretized using the semistructured mesh methodology of Sbardella et al.[31] The basic idea relies on the fact that bladelike structures are not strongly three dimensional because the radial variation is usually small. Therefore, it is possible to start with a structured and body-fitted two-dimensional O grid around a given airfoil section to resolve the boundary layer. This core mesh is then extended in an unstructured fashion up to the far-field boundaries, with the triangulation performed using an advancing front technique. Once this two-dimensional grid is generated, it is projected to the remaining radial sections via quasi-conformal mapping techniques. When all such radial sections are formed, a three-dimensional prismatic grid is obtained by simply connecting the corresponding points of different layers. In this way, hexahedral elements are generated in the viscous region and triangular prisms in the rest of the solution domain.

The meshing of the intake domain is somewhat more complicated and requires two steps.

1) A structured mesh was generated first for the part nearer to the fan. The meshing was done by triangulating the sector of the spinner surface corresponding the fan blade passage, ensuring that it shares the same points with the fan domain at the hub section. The meshes for the fan inflow section and the spinner were projected along the intake duct axis in a structured fashion.

2) The external part of the intake duct mesh was generated using a general-purpose unstructured mesh generator for an intake sector corresponding to a single-blade passage. The duct wall was assumed to be inviscid. This external part has a common boundary with the structured part of the inner domain, and this interface was treated as a sliding boundary in the flow calculations. The external part of the intake mesh was extended about 10 times the intake duct length, taking the shape of a hemisphere toward the far field.

Several views of the mesh for a configuration 1 sector are shown in Fig. 2, where the terminology is also defined. There are about 180,000 points per blade passage, with 30,000 points in the duct domain.

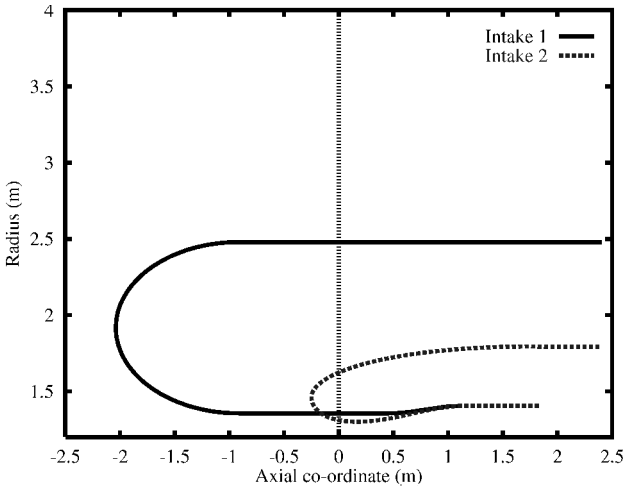

Fig. 1 Comparison of intake geometries for configurations 1 and 2.

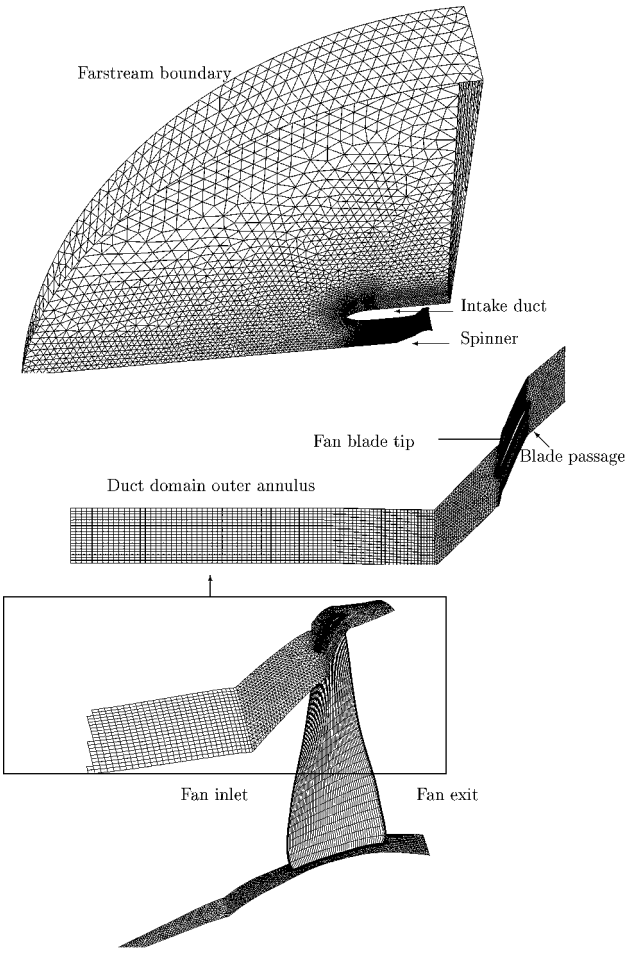

Fig. 2 Views of the viscous sector mesh.

C. Steady-State Flow

The inflow boundary conditions were applied at the farstream of the duct domain, where total pressure and total temperature values were specified at sea-level conditions. A radial pressure distribution was imposed at the outflow of the fan. The aerodynamic conditions used correspond to an elevated working line, which is close to a known flutter boundary. For each speed of interest, the boundary conditions were obtained by linear interpolation from the available data points.

For each configuration, 11 steady-state flow solutions, expressed in a rotating frame of reference, were obtained. The intake duct, being axisymmetric, is also solved in the same rotating frame of reference. A detailed discussion of the flow features at each particular speed is not of primary concern here, and thus, only the general flow features will be discussed in the case of configuration 1.

Figure 3 shows Mach number contours at the tip region of a sector of three blades, an inspection of which reveals the change in fan blade shock position and the propagation of the shock into the intake duct as a function of speed. One of the most important flow

features affecting the flutter behavior is related to the shock position. As typical of modern fan designs, the shock is at the leading edge at low speeds, and it moves farther back toward the trailing edge as the speed increases. At low speeds, the shock is seen to interact with the leading-edge expansion, though it breaks away from it as it moves farther back. From a duct acoustics perspective, 26 such shocks, one on each blade, generate the 26th circumferential mode arising from the first blade passing harmonic. However, note that flutter and its interaction with duct acoustics, and not noise generation due to blade passing harmonic, are of interest here. As will be discussed later, the acoustic modes that interact with flutter behavior arise from the blade vibration and are of much lower order, typically second and third circumferential modes. Similar flow features were obtained for configuration 2, although there are some mass flow rate and pressure ratio differences between the two cases.

The steady-state pressure contours at the periodic boundaries of the analysis sector are shown in Fig. 4 for configuration 1 at 80% speed. As before, the solution is in a rotating frame of reference. As expected, a pressure wave is seen to extend upstream into the intake duct, but its strength is decreasing rapidly at this particular speed.

IV. Flutter Analysis of Configurations 1 and 2

The structural properties of the fan assembly were represented using a linear modal model, with the modes of vibration obtained from a standard finite element code. The assembly modes corresponding to the first three blade modes were included in the flutter analysis. The first bending mode shape of the blade, the first flap 1*F* mode, is plotted in Fig. 5. The contour levels indicate the amount of vibratory motion, with the tip section exhibiting the largest response.

From the outset, it was decided to perform a whole-assembly flutter analysis and not to use the cyclic symmetry. Such an approach

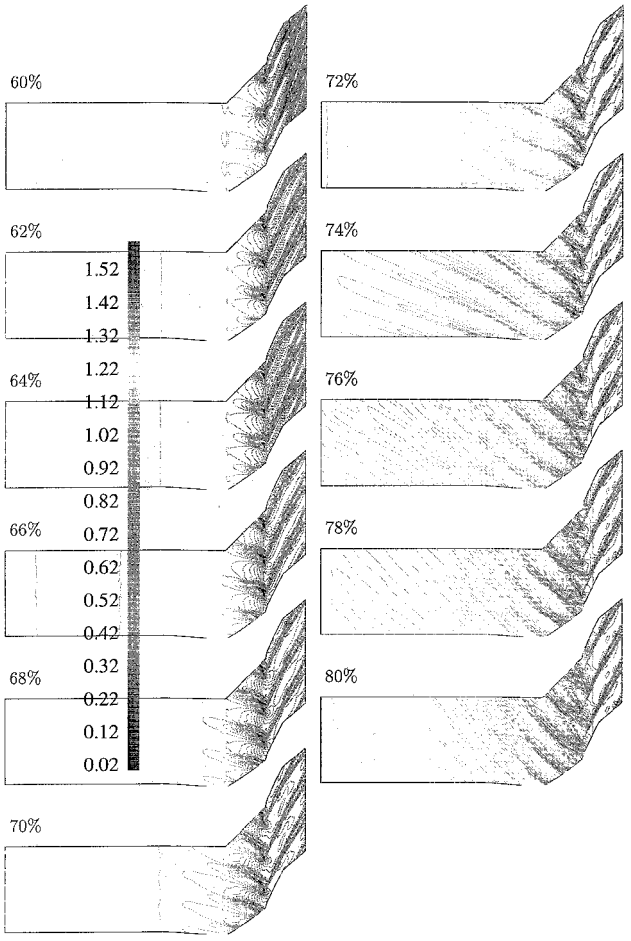

Fig. 3 Mach contours at blade tip–three-bladed sector, configuration 1.

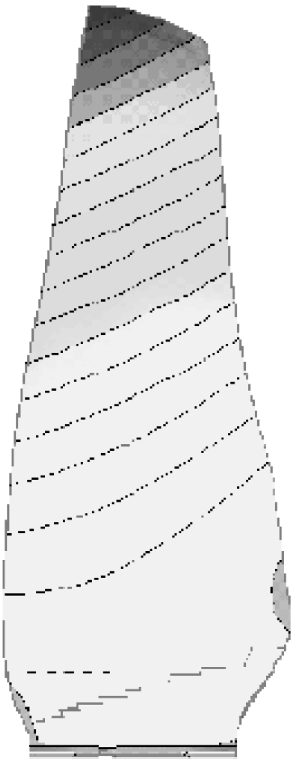

Fig. 5 At 70% speed, 1*F* mode shape.

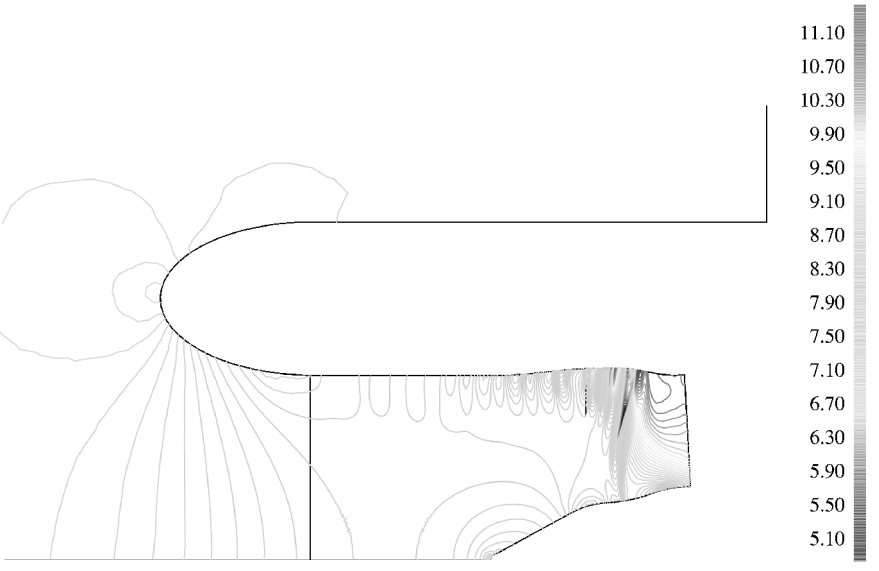

Fig. 4 Pressure contours at the periodic boundary for 80% speed, configuration 1.

not only circumvents guessing the unstable nodal diameter modes, but also allows interactions between the vibration modes. Given the excessive computational requirements for a viscous nonlinear time-accurate unsteady flow simulation with a full assembly, it was decided to use an inviscid flow representation coupled to a loss model. In the present work, the loss model was defined numerically using data from the previous viscous single-passage steady-state flow analyses. A coarser mesh with about 30,000 points per blade passage was created, and the available single-passage viscous solutions were extrapolated onto this coarser mesh for each speed of interest. The viscous stresses of the first solution are, thus, saved on the second mesh and used throughout the unsteady inviscid solution as source terms. The total number of mesh points was about 900,000 for each individual whole-assembly flutter analysis with an inviscid plus loss model flow representation.

A. Results and Discussion

The flutter calculations were started by giving initial modal velocities to all modes included in the computations, a numerical procedure that is analogous to hitting a blade and monitoring whether the response is decaying or growing in time.

For each configuration, 11 flutter calculations were undertaken and typical modal time histories are plotted in Fig. 6. The unstable modes have growing time histories, whereas the stable ones have decaying ones. As can be seen from Fig. 6a, the two-nodal-diameter (ND) mode at 68% speed is unstable for configuration 1 and stable for configuration 2. Similarly, the growing time history of Fig. 6b indicates an unstable three-ND mode at 74% speed for configuration 1, whereas the same mode is stable in configuration 2, as indicated by the much lower response (almost indistinguishable from the x axis in Fig. 6b). Finally, Fig. 6c indicates that the five-ND mode is stable for both configurations at 74% speed.

For each time history, it is possible to calculate a logarithmic decrement (logdec) value, that is, the decay rate between two given cycles in the time history. In flutter calculations, it is customary to assume zero structural damping; hence, the logdec value is representative of the aerodynamic damping only. After processing the modal time histories in this fashion, the aerodynamic damping in the two-ND modes was plotted as a function of speed for both configurations (Fig. 7). When it is recalled that both configurations have the same nominal fan assembly running to identical aerodynamic conditions, the difference in the flutter behavior can only be due to the intake duct properties. It is seen that the aerodynamic damping, indicated by the logdec value to some datum level, is strongly speed dependent, although there are less discrepancies for both ends of the speed range. The aerodynamic damping plots exhibit sharp drops at some specific speeds, which indicates that the flutter stability is greatly reduced for very narrow speed ranges. In any case, the striking finding is the very significant effect of the intake duct geometry on flutter stability.

When ranking the intakes for flutter stability, what is of interest is the variation of the least stable mode with speed. The findings of such an investigation are summarized in Fig. 8, where the least stable nodal diameter mode is indicated for each speed. For both configurations, the two-ND mode is generally the least stable one. Note the least stable mode is not necessarily the same across the speed range. For instance, at 66% speed, the least stable ND mode is two for configuration 1 and four for configuration 2.

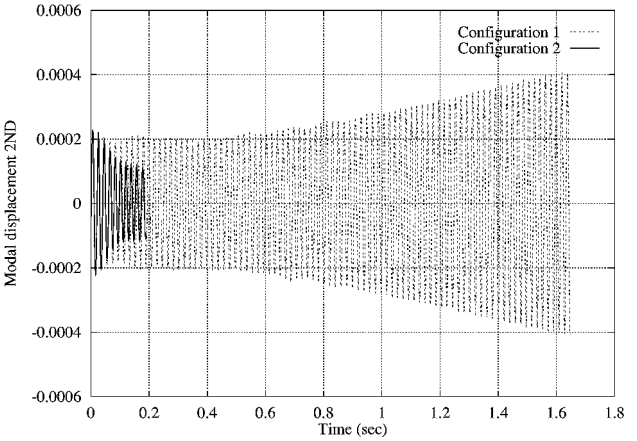

a) 2ND at 68% speed

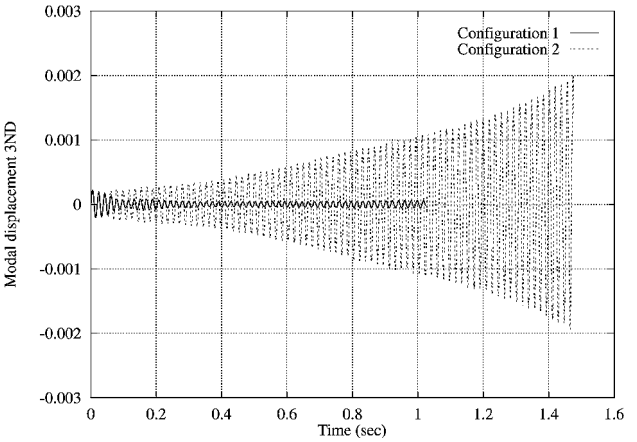

b) 3ND at 74% speed

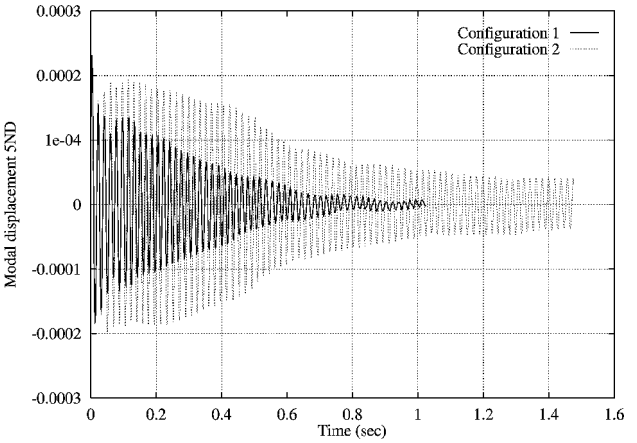

c) 5ND at 74% speed

Fig. 6 Typical modal displacement time histories; larger-amplitude time history, either configuration, shown in lighter dotted line.

B. Viscous Flutter Analysis of Intake 2

The single-passage viscous mesh used for the steady-state flow analysis of configuration 2 was expanded to discretize the whole fan assemby plus intake 2, although the latter was modeled inviscidly. The discretization of such geometries is relatively straightforward with an unstructured CFD mesh, which not only offers great modeling flexibility but also allows different grid densities in various parts of the computational domain. The final mesh contained about 3.6×10^6 points, and the memory requirement to undertake flutter calculations with moving meshes was about 2 GB. Each flutter run consisted of computing the first 10 cycles of vibration, with each cycle having about 100 time steps. The computing time was about 50 days on a single 600-MHz 21164 DEC Alpha processor, although the current generation of the same CPU (21264) is about four times faster at the same clock speed, and hence, the time may be expected to reduce to 12.5 days. In any case, at the time of conducting the analysis, it was not possible to undertake a large number of such computations within realistic timescales, and it was decided to perform the viscous flutter computations at one speed only, with the aim being to verify the accuracy of the earlier inviscid plus loss model computations.

A comparison of inviscid and viscous flutter analyses of configuration 2 at 66% speed can be seen from the standard stability vs nodal diameter mode diagram of Fig. 9. It can be seen that there is a good agreement between the inviscid and viscous flutter models; the same nodal diameters modes are predicted as unstable by both approaches. Some of the discrepancies are because the damping values, which were computed from nonlinear time histories, are

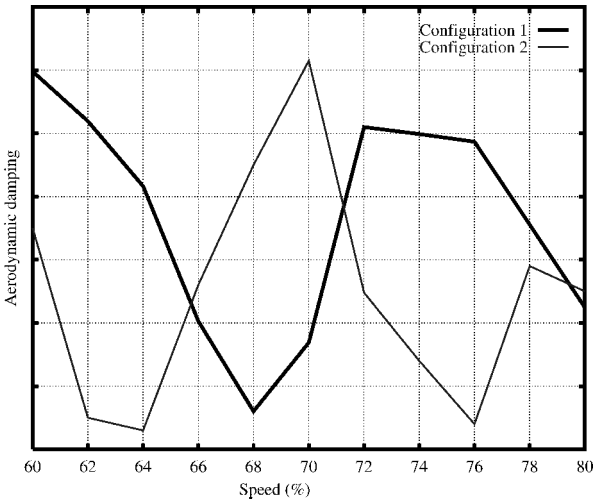

Fig. 7 Aerodynamic damping vs speed (%) for configurations 1 and 2; two-ND mode.

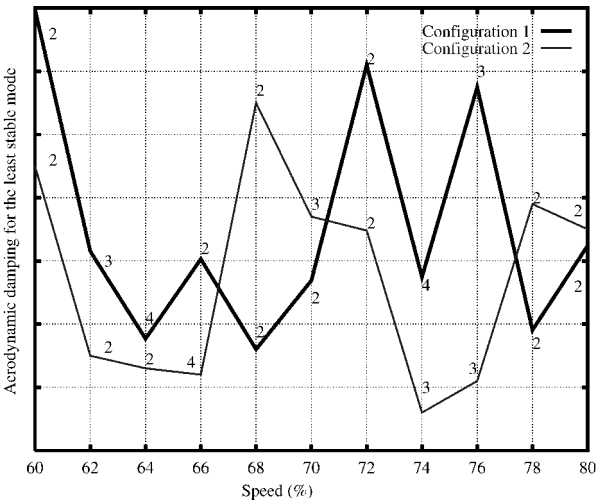

Fig. 8 Least stable mode vs speed %.

somewhat sensitive to the definition of the starting and finishing cycles when computing the log dec. Fortunately, such discrepancies are much more pronounced for stable modes, and the agreement for the least stable region of two-ND to five-ND modes is good.

C. Unsteady Pressure Perturbation due to Fan Assembly Vibration

During the flutter computations, the instantaneous pressure perturbations were recorded at each time instant at some duct radius close to the fan face. Such a circumferential distribution is shown in Fig. 10 for configuration 2 running at 74% speed. A spatial Fourier transform of this distribution will reveal the harmonics of the pressure perturbation due to the blade motion. Successive Fourier transforms of such instantaneous perturbations will yield a time history for each harmonic, and these can then be compared to the modal time histories of the blade motion to assess the relationship between the blade motion and the ensuing pressure perturbation. Two Fourier transforms of the instantaneous pressure distributions, after 10 and 15 vibration cycles, respectively, are plotted in Fig. 11. The analysis shows a strong time-varying third harmonic, indicating that the fan is, in the main, vibrating in a three-ND mode (Fig. 11).

By means of successive Fourier transforms taken at different time steps during the vibration cycle, the unsteady pressure and velocity

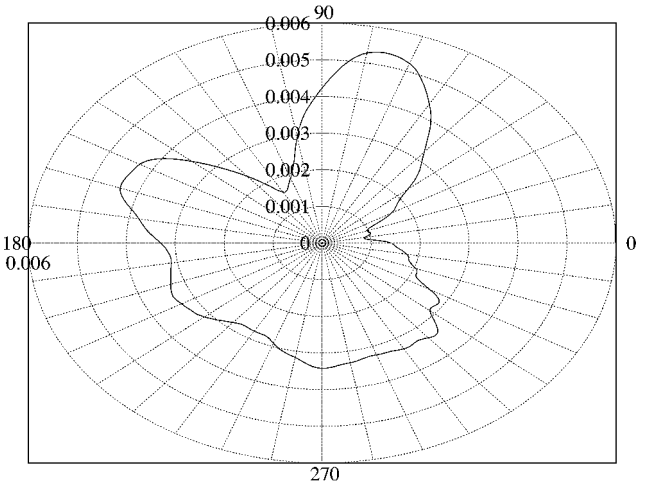

Fig. 10 Circumferential pressure fluctuation, configuration 2 at 74% speed.

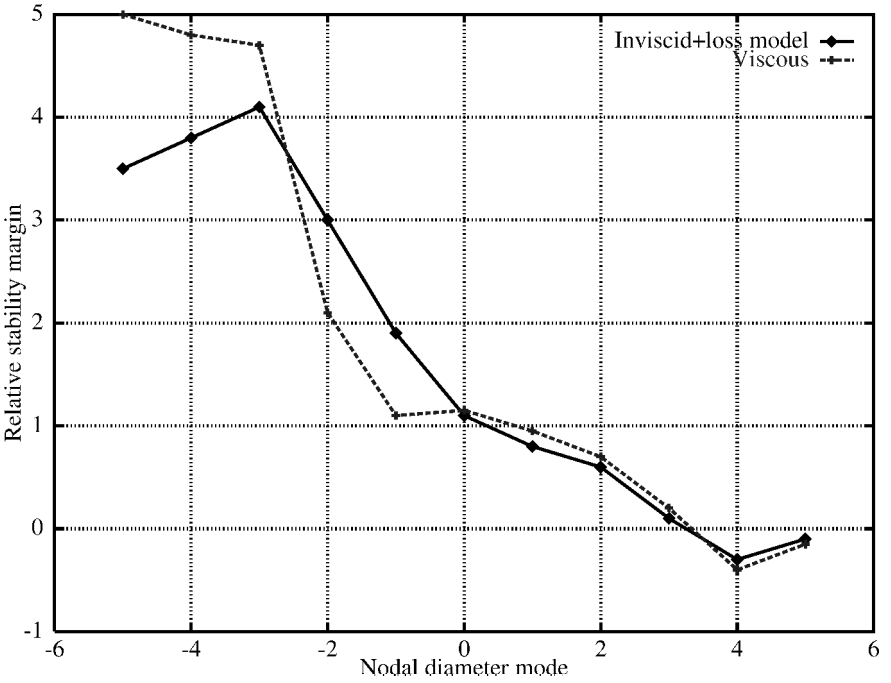

Fig. 9 Aerodynamic damping at 66% speed.

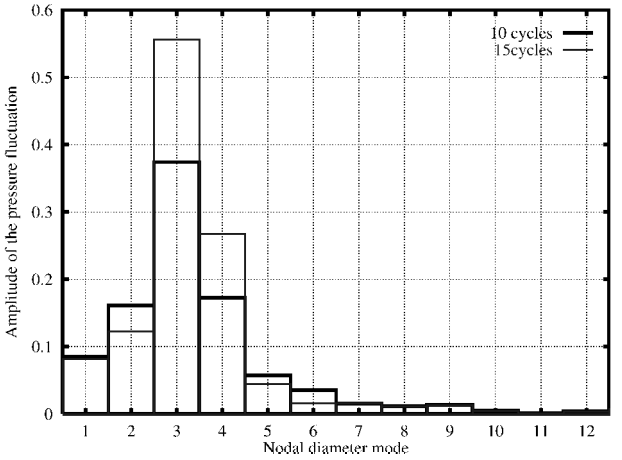

Fig. 11 Pressure harmonics after 10 and 15 vibration cycles, configuration 2.

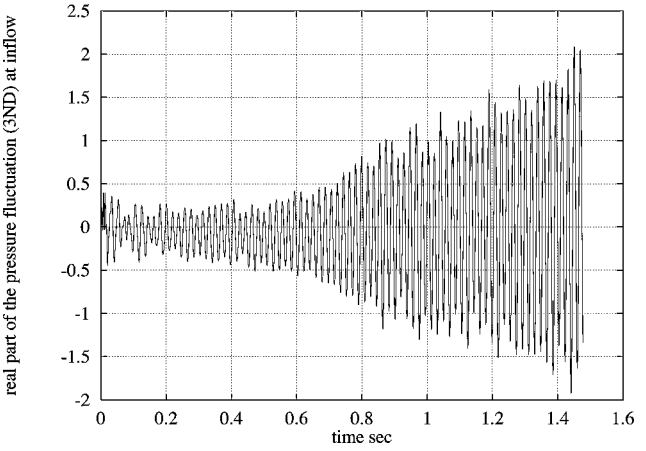

Fig. 12 Real part of the three-ND pressure fluctuation at inflow, 74% speed.

time histories can be obtained for each ND harmonic. Such unsteady pressure harmonics are plotted in Fig. 12, from which the unstable behavior of three-ND/74% speed/configuration 2 can easily be seen from the growing time history. On the other hand, the two-ND mode/76% speed/configuration 1 has a decaying time history (not shown), indicating stable behavior. A comparison of Figs. 12 and 6b reveals that the pressure perturbation follows the blade motion closely. This finding will be exploited when constructing a simplified model in Sec. VI. The pressure perturbations are, thus, consistent with the previous results obtained from the actual vibration time histories. Three conclusions can be drawn from this analysis:

1) Growing blade vibration amplitude in a given nodal diameter mode and growing unsteady pressure in the corresponding harmonic are closely linked, although the exact mechanism is, so far, unclear.

2) The instantaneous pressure perturbations contain several harmonics, which indicates the possibility of flutter occurring in several nodal diameter modes simultaneously.

3) The pressure perturbation created by the fan vibration may be viewed as an excitation source for the acoustic modes of the intake duct. Such a possibility will now be investigated in more detail.

V. Investigation of the Flutter Mechanism

A. General Considerations

From the results, it is clear that the interaction of duct acoustics with the unsteady oncoming pressure perturbation from the fan is one of the key factors in understanding the flutter stability. The flutter modes rotate in the same direction as the fan, that is, the instability occurs in forward-traveling ND modes. When it is noted that the flow swirl due to the fan is also in the same direction, it may be speculated that a marginally cuton acoustic mode that is ahead of the fan may become cutoff downstream because of the effects of the swirling flow. Consequently, the acoustic wave number and assembly mode combinations, which produce propagating modes ahead of the fan and decaying modes at the throat, can also produce decaying modes behind the fan. Such a hypothesis implies that the acoustic energy generated at the fan face may become trapped in the intake. This effect is illustrated in the schematic diagram of Fig. 13. The possible flutter frequencies of a generic fan are plotted as a function of the engine speed, along with the cuton frequencies of the possible acoustic modes. The acoustic cuton frequencies are different at the fan and the throat, and so both frequencies are plotted at each engine speed. The aim of Fig. 13 is to show that, for representative intakes, resonance may occur at part speed flutter with low, positive nodal diameter numbers. Figure 13 may be considered to be the equivalent of a Campbell diagram, which is commonly used for rotor–stator forced response evaluations. As for forced response, there must be both frequency and shape match between a structural ND mode and an acoustic mode. For instance, referring to Fig. 13, a two-ND vibration mode of the fan assembly may be considered to be a $\cos 2\theta$ wave, and the resulting unsteady pressure pressure of the same shape will excite an acoustic mode whose circumferential wave number is also $m = 2$. Furthermore, for a particular phase relationship between the unsteady pressure field generated at the fan

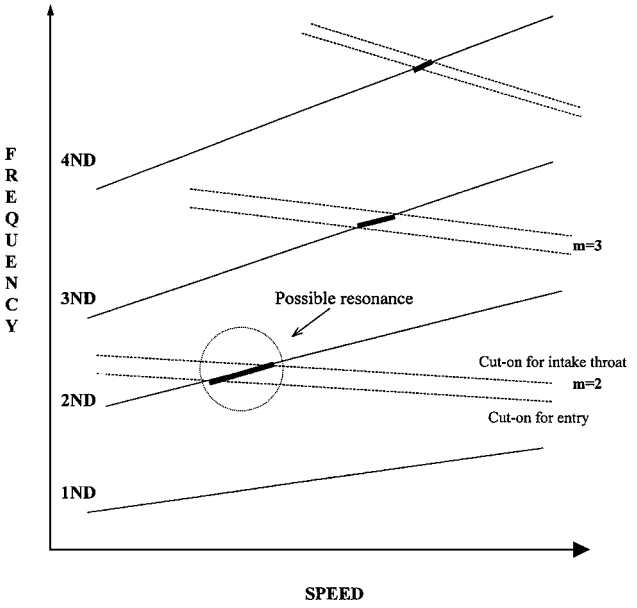

Fig. 13 Matching between intake acoustic modes and blade flutter frequencies.

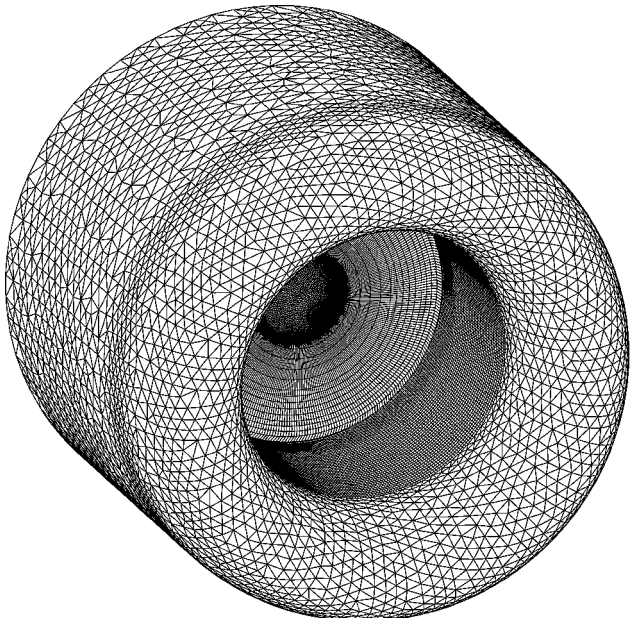

Fig. 14 Prescribed unsteady two-ND pressure and resulting velocity profiles.

and that reflected from the intake throat, the flutter behavior will be exacerbated by the successive reflections of the trapped energy. In any case, the overall dynamic behavior can be described as an impedance match between the pressure perturbation created by the fan and the acoustic response of the duct. Such a scenario will now be simulated by focusing on the intake duct only.

B. Simplified Model for Fan Perturbation

One way of studying the acoustic impedance match between the duct and the fan assembly is to consider the transfer function between the (input) unsteady pressure due to the fan and the (output) axial velocity perturbations in the duct. By changing the rotational speed, that is, the frequency of the rotating disturbance due to the fan, one can characterize the acoustic behavior of the duct in terms of a frequency response function. Such an approach will be adopted here.

The pressure fluctuation due to the presence of a rotating fan with vibrating blades is given by

$$p = A\bar{p}(r)\sin[N\theta + (\omega_b + N\Omega)t] \tag{1}$$

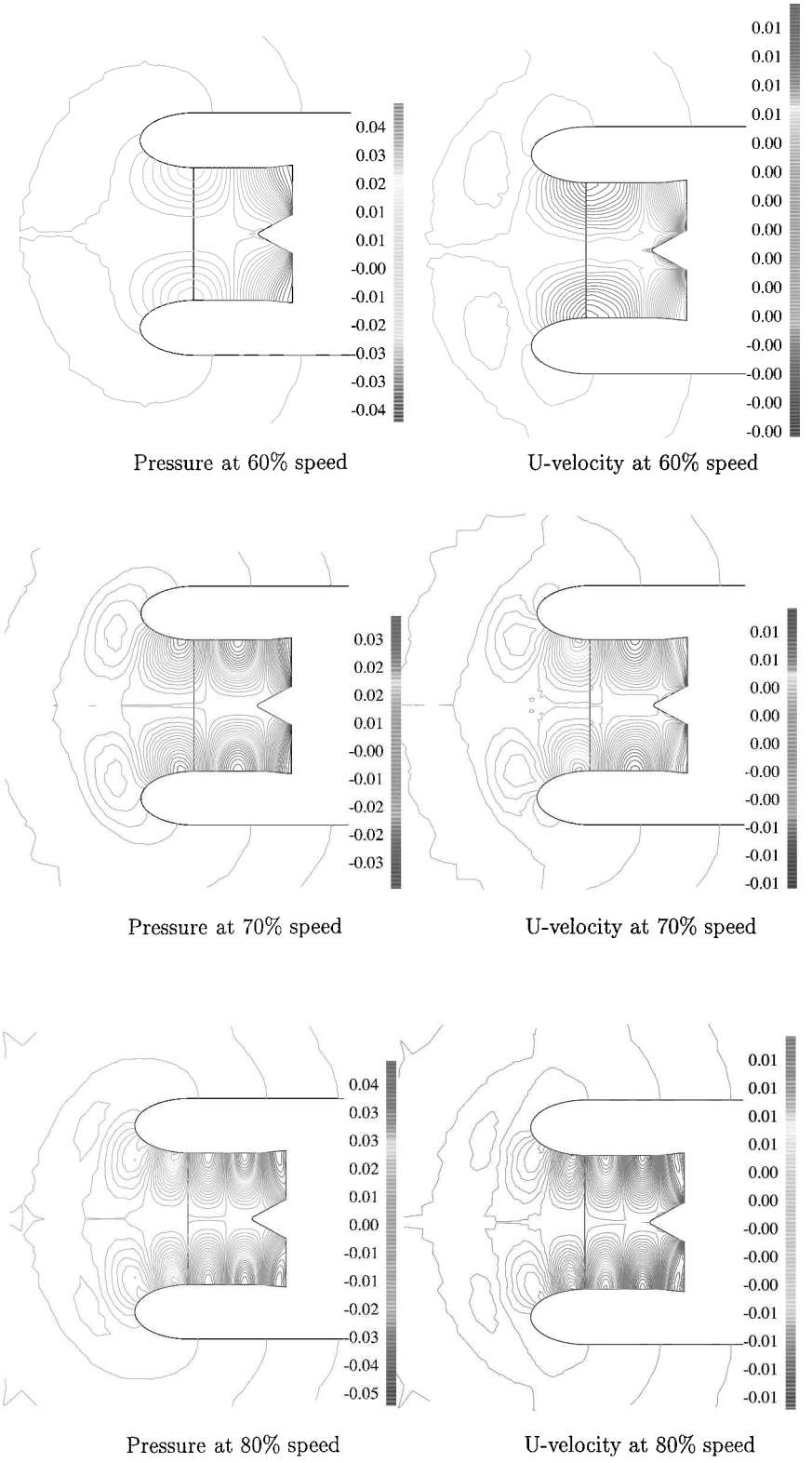

Fig. 15 Two-ND unsteady pressure and axial velocity profiles at different speeds.

where $\bar{p}(r)$ is the steady-state pressure as a function of the radial coordinate r and N is the ND number of the vibration mode, Note that the perturbation is defined as a percentage of the steady-state pressure distribution, which has a radial variation.

Such a simplified model has a number of limitations:

1) Any changes to the fan flutter condition due to acoustic interactions from the intake duct are not modeled because the pressure perturbation is kept fixed throughout the calculations.

2) The model does not prevent the acoustic energy from the intake from escaping downstream, whereas, in the real case, the presence of swirling flow behind the fan will largely prevent such a leak. In any case, the real situation is likely to be much more complicated due to outlet guide vane and pylon effects.

C. Aeroacoustic Calculations for Intake 1

The computational grid, shown in Fig. 14, was obtained by removing the fan blade from the earlier mesh used for the inviscid plus loss model flutter calculations. Standard external flow boundary conditions were used at the far field. For the steady-state flow computations, the mean static pressure was imposed at the duct exit.

Steady-state flow solutions were obtained first for all 11 speeds of interest. The computed mass flow rates were found to be comparable to those obtained earlier for the complete geometry. To cover all 11 speeds for the two-, three-, and four-ND modes, 33 separate unsteady aeroacoustic calculations were performed. For a given $1F$ natural frequency, the frequency of the perturbation due to fan rotation and blade vibration is given by

$$\omega = \omega_b + N\Omega \tag{2}$$

The values obtained from Eq. (2) for the particular case under study are listed in Table 1.

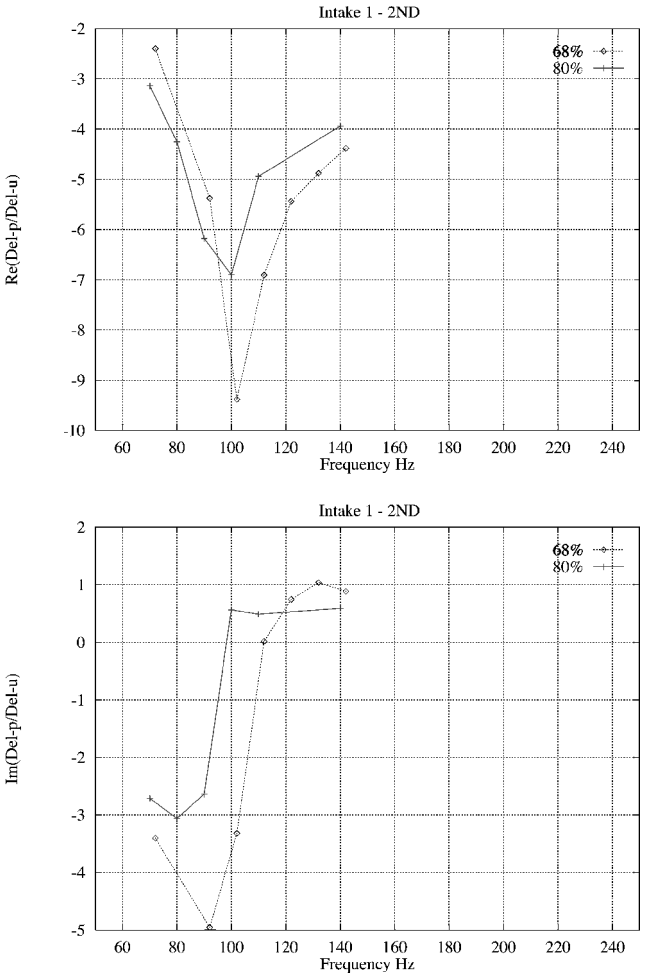

Fig. 16 Real and imaginary parts of $\Delta p/\Delta u$ at inflow for two-ND, 68 and 80% speed.

Table 1 Fan perturbation frequencies

	Frequency for ND mode:		
Speed, %	2	3	4
60	111.10	142.22	173.33
62	114.00	146.16	178.33
64	116.85	150.05	183.25
66	119.70	153.92	188.15
68	122.56	157.83	193.09
70	125.44	161.74	198.04
72	128.31	165.65	202.99
74	131.18	169.55	207.93
76	134.05	173.46	212.88
78	137.05	177.50	217.95
80	139.78	181.27	222.75

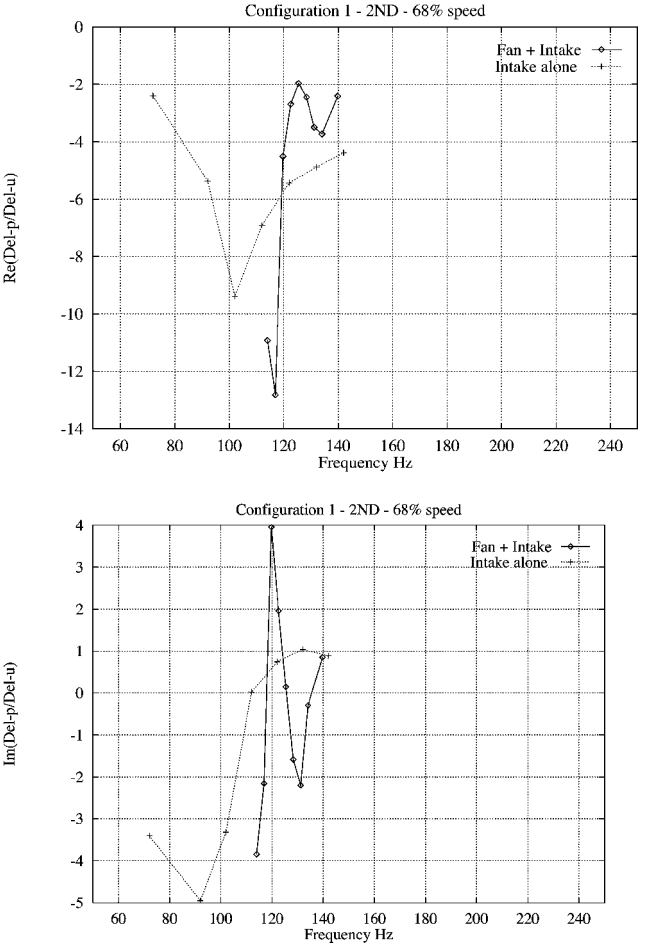

Fig. 17 Real and imaginary parts of $\Delta p/\Delta u$ at inflow for two-ND, intake alone vs full configuration.

For the unsteady aeroacoustic calculations, Eq. (1) was applied at the duct exit as a boundary condition. The amplitude of the pressure perturbation, $\bar{p}$, was set to 5% of the steady-state value, and this was added to the steady-state pressure at the fan inlet. The propagation of both the unsteady pressure and of the corresponding axial velocity perturbation were monitored at several speeds along the duct length. Such data are plotted in Fig. 15 for 60, 70, and 80% speeds. It is seen that, for the two-ND mode, the pressure wave is cuton (propagating) for the 70–80% speed range and cutoff (decaying) for the 60–70% speed range. Clearly, the duct is exibiting markedly different behavior between these two cases, one giving rise to a flutter condition and the other remaining stable. To gain further insight, the cases of 68% speed/two-ND mode (unstable) and 80% speed/two-ND mode (stable) were analyzed in more detail. A frequency sweep using Eq. (1) was performed for these conditions by changing the excitation frequency ω of Eq. (2). The cuton frequency was determined by monitoring the behavior of the unsteady pressure wave along the duct. This critical value was found to be 107 Hz for the

Table 2 Duct-alone and full configuration flutter conditions

Flutter condition	68% speed/two-ND (unstable)
Duct-alone cuton frequency	107 Hz
Full configuration cuton frequency	118 Hz
Critical perturbation frequency from Table 1	122 Hz

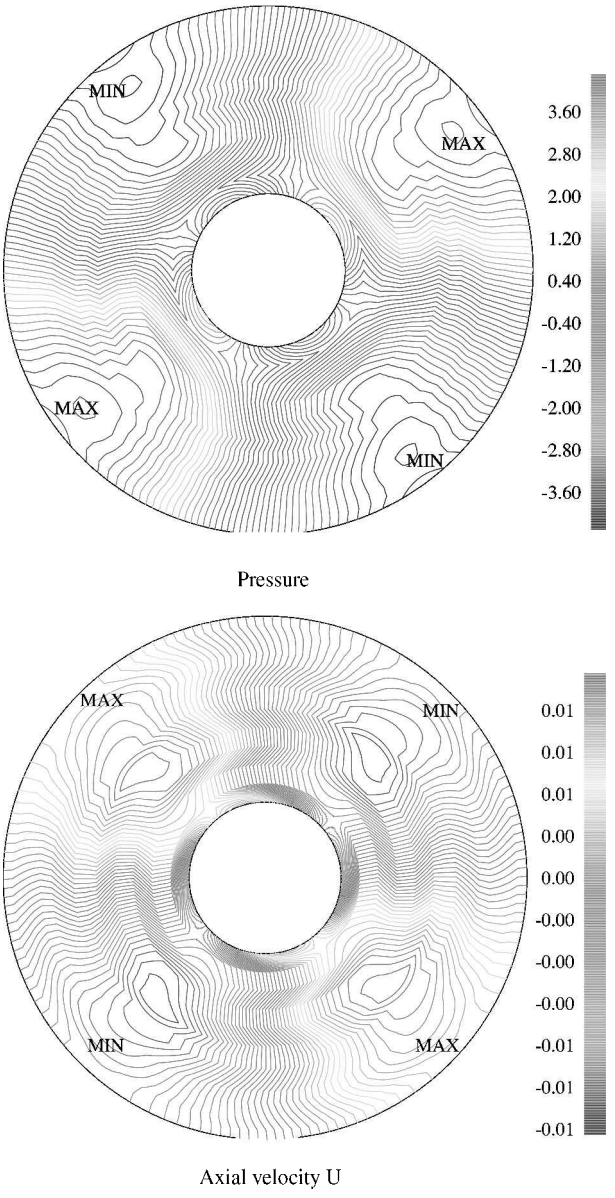

Fig. 18 Unsteady pressure and velocity profiles at 68% speed, configuration 1/two ND (unstable).

two-ND/68% speed case, and 100 Hz for the two-ND/80% speed case. For 80% speed, an excitation frequency of 100 Hz will correspond to a blade frequency ω_b of 12 Hz. Given that the actual blade frequency is 52.8 Hz, the fan cannot produce a perturbation at the critical frequency of 100 Hz at 80% speed. However, for the two-ND/68% speed case, the duct cuton frequency of 107 Hz is quite close to two-ND/68% speed of 122 Hz of Table 1. This frequency matching is thought to be a prime reason for the occurrence of flutter at 68% speed.

The behavior of the duct can be studied further by monitoring its acoustic impedance parameter, which is the ratio of unsteady pressure to unsteady axial velocity. As before, the required data were obtained by successive Fourier transforms of the pressure and velocity time histories for each excitation frequency. Figure 16 shows the real and imaginary parts of the intake 1/two-ND impedance for 68 and 80% speeds. It is seen from the real part plot that there is a significant magnitude increase near the cuton conditions of 100 Hz (80% speed) and 107 Hz (68% speed). As discussed earlier, the perturbation from the fan can match the cuton frequency at 68% speed, but not at 80% speed. After the cuton condition, the imaginary part of the impedance becomes nearly zero, indicating that velocity and pressure perturbations are out of phase. The results agree very well with those obtained by T. Hynes (private communication, 1988) for a generic duct.

VI. Reconciliation of Full Configuration and Intake-Alone Results

The output from the earlier full configuration runs was postprocessed in the same fashion, and the results are compared to intake-alone ones in Fig. 17. A summary of the relevant numerical data is given in Table 2.

An inspection of Fig. 17 reveals that the impedance behavior of the full configuration is very similar to that of duct-alone case, but there is a shift of about 10% between the two cuton frequencies. For the 68% speed/two-ND case, flutter occurs when the excitation frequency of 122 Hz is near the cuton frequency of 107 Hz (duct alone) or 118 Hz (full configuration).

Finally, a further critical feature was observed to be the phase difference between the pressure perturbation and the axial velocity perturbation. The full-assembly computations include all possible NDs and, hence, the study of a particular ND requires a Fourier decomposition, filtering of all other nodal diameters, and resynthesis for the ND of interest. The unsteady pressure and velocity plots at the fan inflow plane are given in Fig. 18 for the unstable case of the two-ND mode at 68% speed. The unsteady pressure and the resulting unsteady velocity are almost out of phase, the minimum of the velocity pattern occurring slightly earlier than the maximum of the corresponding pressure pattern. On the other hand, the behavior is stable for the case of 68% speed/three-ND mode (not shown). The two quantities are no longer out of phase; this time the minimum of the velocity perturbation occurs well after the maximum of the pressure perturbation.

VII. Conclusions

1) During rig testing of development engines, sudden reductions in flutter margin may occur for very narrow speed ranges. It has been possible to simulate such observed behavior using an integrated aeroelasticity model of a whole-annulus fan assembly and intake duct. The flutter bite was shown to consist of several sharp drops, each arising from an acoustic mode of the duct. During the numerical simulations, inherent mechanical damping was assumed to be zero, and although its inclusion will improve the overall stability, the general trend is likely to remain the same.

2) Flutter occurs when the pressure perturbation due to fan rotation and blade vibration matches, both in frequency and shape, an acoustic mode of the intake. The critical frequency of the fan perturbation is seen to be the blade frequency in the rotating frame of reference, and this can be computed using Eq. (2). The associated critical shape is the nodal diameter vibration pattern of the fan assembly.

3) It is concluded that a full description of the flutter instability needs to include an intake model. The presence of multiharmonics in the instantaneous pressure perturbations due to the fan rotation indicates the possibility of modal interactions during flutter.

4) The flutter margin was predicted to be much higher with the straight intake than with the symmetric flight intake. This is consistent with acoustic reflections being significantly more important for the flight intake because of its variable cross section and shorter length.

5) A large number of intake-alone calculations were performed to obtain the acoustic frequency response of the duct to a simulated fan perturbation. The duct's acoustic behavior was characterized by its frequency response, from which the acoustic mode cuton frequencies were obtained. Flutter occurred each time the combination of the blade frequency, the number of NDs, and the rotational speed matched this cuton frequency.

6) At the design stage, instability may be inferred from an inspection of the duct-alone cuton frequencies and the critical perturbation frequencies of the fan assembly. However, full-assembly plus duct and duct-alone cuton frequencies were seen to differ by as much as 10%. Therefore, it may be difficult to assess the stability of certain speed/ND combinations without a full analysis.

7) The findings also support the view that mistuning is beneficial for flutter stability. The existence of mistuning will cause the pure ND patterns to degenerate, and hence, the matching of the shape of an acoustic mode will be more difficult. Acoustic liners and upstream obstacles may also play a similar role.

8) The flutter results from the two modeling levels, that is, viscous or inviscid plus loss model, were found to be in good agreement. Therefore, the inviscid flow plus loss model representation seems to be adequate to predict the global characteristics of fan assembly flutter with an intake duct. The generalization of this observation requires the study of further cases.

Acknowledgments

The authors would like to thank Rolls–Royce, plc., for both sponsoring this work and allowing its publication. They gratefully acknowledge the contribution of their colleagues at Rolls–Royce: C. Freeman, D. Halliwell, J. G. Marshall, J. W. Chew, R. M. Hall, and A. B. Parry. They also acknowledge many useful discussions with N. Cumpsty and T. Hynes of Cambridge University.

References

[1]Marshall, J. G., and Imregun, M., "A Review of Aeroelasticity Methods with Emphasis on Turbomachinery Applications," *Journal of Fluids and Structures*, Vol. 10, No. 3, 1996, pp. 237–267.

[2]Kielb, R. E., and Ramsey, J. K., "Flutter of a Fan in Supersonic Axial Flow," *Journal of Turbomachinery*, Vol. 111, No. 2, 1989, pp. 461–471.

[3]Smith, T. E., and Kadambi, J. R., "The Effect of Steady Aerodynamic Loading on the Flutter Stability of Turbomachinery Blading," American Society of Mechanical Engineers, ASME Paper 91- GT-130, 1991.

[4]Imregun, M., "Prediction of Flutter Stability Using Aeroelastic Response Functions," *Journal of Fluids and Structures*, Vol. 9, No. 5, 1995, pp. 419–434.

[5]Guruswamy, G. P., and Goorjian, P. M., "Unsteady Transonic Aerodynamics and Aeroelastic Calculations at Low Supersonic Freestreams," *Journal of Aircraft*, Vol. 25, 1988, pp. 955–967.

[6]Bakhle, M. A., Reddy, R., and Keith, T. H., "Time Domain Flutter Analysis Using a Potential Solver," *AIAA Journal*, Vol. 30, No. 1, 1992, pp. 163–173.

[7]Chew, J. W., Vahdati, M., and Imregun, M., "Predicted Influence of Intake Acoustics upon Part-speed Flutter," American Society of Mechanical Engineers, ASME Paper 98-GT-558, 1998.

[8]Vahdati, M., Sayma, A. I., Marshall, J. G., and Imregun, M., "Mechanisms and Prediction Methods for Fan Blade Stall Flutter," *Journal of Propulsion and Power*, Vol. 17, No. 5, 2001, pp. 1100–1108.

[9]Campos, L. M. B. C., and Lau, F. J. P., "On the Acoustics of Low Mach Number Bulged, Throated and Baffled Nozzles," *Journal of Sound and Vibration*, Vol. 196, No. 5, 1996, pp. 611–633.

[10]Uenishi, K., and Myers, M. K., "Two-Dimensional Acoustic Field in a Nonuniform Duct Carrying Compressible Flow," *AIAA Journal*, Vol. 22, No. 7, 1984, pp. 1242–1248.

[11]Eversman, W., and Astley, R. J., "Acoustic Transmission in Nonuniform Ducts with Mean Flow. Part I: The Method of Weighted Residuals," *Journal of Sound and Vibration*, Vol. 74, No. 1, 1981, pp. 89–101.

[12]Astley, R. J., and Eversman, W., "Acoustic Transmission in Nonuniform Ducts with Mean Flow. Part II: The Finite Element Method," *Journal of Sound and Vibration*, Vol. 74, No. 1, 1981, pp. 103–121.

[13]Nayfeh, A. H., Kaiser, J. E., and Telionis, D. P., "Transmission of Sound Through Annular Ducts of Varying Cross Sections," *AIAA Journal*, Vol. 13, No. 1, 1975, pp. 60–65.

[14]Nayfeh, A. H., Kaiser, J. E., and Shaker, B. S., "A Wave Envelop Analysis of Sound Propagation in Non-uniform Circular Ducts with Compressible Mean Flows," NASA CR 3109, 1979.

[15]Nayfeh, A. H., Shaker, B. S., and Kaiser, J. E., "Transmission of Sound Through Nonuniform Circular Ducts with Compressible Mean Flows," *AIAA Journal*, Vol. 18, No. 3, 1980, pp. 515–525.

[16]Hanson, D. B., "Mode Trapping in Coupled Two-Dimensional Cascade: Acoustic and Aerodynamic Results," AIAA Paper 93-4417, 1993.

[17]Smith, S. N., "Discrete Frequency Generation in Axial Flow Turbomachines," Aeronautical Research Council, Repts. and Memoranda 3079, London, 1972.

[18]Eversman, W., "Mapped Infinite Wave Envelope Elements for Acoustic Radiation in a Uniformly-Moving Medium," *Journal of Sound and Vibration*, Vol. 224, 1999, pp. 665–687.

[19]Astley, R. J., "Infinite Elements for Wave Problems: A Review of Current Formulations and an Assessment of Accuracy," *International Journal for Numerical Methods in Engineering*, Vol. 17, No. 7, 2000, pp. 31–41.

[20]Ozyoruk, Y., and Long, L. N., "Computation of Sound Radiating from Engine Inlets," *AIAA Journal*, Vol. 34, No. 5, 1996, pp. 894–901.

[21]Ozyoruk, Y., and Long, L. N., "Multigrid Acceleration of a High-Resolution Computational Aeroelastics Scheme," *AIAA Journal*, Vol. 35, No. 3, 1997, pp. 428–433.

[22]Rumsey, C. L., Biedron, R. T., Farassat, F., and Spence, P. L., "Ducted-Fan Engine Acoustic Predictions Using a Navier–Stokes Code," *Journal of Sound and Vibration*, Vol. 213, No. 4, 1998, pp. 643–664.

[23]Melling, T. H., "The Acoustic Impedance of Perforates at Medium and High Sound Pressure Levels," *Journal of Sound and Vibration*, Vol. 29, No. 1, 1973, pp. 1–65.

[24]Tester, B. J., "Some Aspects of Sound Attenuation in Lined Ducts Containing Inviscid Mean Flows with Boundary Layers," *Journal of Sound and Vibration*, Vol. 28, No. 2, 1973, pp. 217–245.

[25]Sbardella, L., Tester, B. J., and Imregun, M., "The Attenuation of Sound in a Lined Duct Using a Time-Domain Simulation," *Journal of Sound and Vibration*, Vol. 239, No. 3, 2001, pp. 379–396.

[26]Vahdati, M., and Imregun, M., "A Non-Linear Integrated Aeroelasticity Analysis of a Fan Blade Using Unstructured Dynamic Meshes," *Journal of Mechanical Engineering Science*, Pt. C, Vol. 210, No. 5, 1996, pp. 549–563.

[27]Sayma, A. I., Vahdati, M., and Imregun, M., "Multi-stage Whole-Annulus Forced Response Predictions Using an Integrated Non-linear Analysis Technique Part I: Numerical Model," *Journal of Fluids and Structures*, Vol. 14, No. 1, 2000, pp. 87–101.

[28]Sayma, A. I., Vahdati, M., Sbardella, L., and Imregun, M., "Modelling of Three-Dimensional Viscous Compressible Turbomachinery Flows Using Unstructured Hybrid Grids," *AIAA Journal*, Vol. 38, No. 6, 2000, pp. 945–954.

[29]Rumsey, C. L., Sanetrik, M. D., Biedron, R. T., Melson, N. D., and Parlette, E. B., "Efficiency and Accuracy of Time-Accurate Turbulent Navier–Stokes Computations," *Computers and Fluids*, Vol. 25, No. 2, 1996, pp. 217–236.

[30]Sayma, A. I., Vahdati, M., Green, J. S., and Imregun, M., "Whole-Assembly Flutter Analysis of a Low Pressure Turbine Blade," *Aeronautical Journal*, Vol. 102, No. 1018, 1998, pp. 459–463.

[31]Sbardella, L., Sayma, A. I., and Imregun, M., "Semi-structured Meshes for Axial Turbomachinery Blades," *International Journal for Numerical Methods in Fluids*, Vol. 32, No. 4, 2000, pp. 569–584.

E. Livne
Associate Editor